Controllable Synthesis of Silver Nanoparticle Aggregates for Surface-Enhanced Raman Scattering Studies

ARTICLE *in* THE JOURNAL OF PHYSICAL CHEMISTRY C · JULY 2011

Impact Factor: 4.77 · DOI: 10.1021/jp205545g

7 AUTHORS, INCLUDING:

Lanlan Sun
Chalmers University of Technology
46 PUBLICATIONS **917** CITATIONS

SEE PROFILE

THE JOURNAL OF PHYSICAL CHEMISTRY C

ARTICLE

pubs.acs.org/JPCC

Controllable Synthesis of Silver Nanoparticle Aggregates for Surface-Enhanced Raman Scattering Studies

Lanlan Sun, Dongxu Zhao,* Meng Ding, ZhiKun Xu, Zhenzhong Zhang, Binghui Li, and Dezhen Shen

Key Laboratory of Excited State Processes, Chinese Academy of Sciences, Changchun Institute of Optics, Fine Mechanics and Physics, Chinese Academy of Sciences, 16 East Nan-Hu Road, Open Economic Zone, Changchun 130033, People's Republic of China

Supporting Information

ABSTRACT: Aggregation of citrate-reduced silver nanoparticles (Ag nps) induced by cetyltrimethylammonium bromide (CTAB) was studied by UV−vis absorption spectra, SEM, and zeta potential measurement. Subsequently, Rhodamin 6G (R6G) and 4-aminothiophenol (4-ATP) were used for testing the SERS activity on these aggregates with very low concentrations, and it was found that the enhancement ability was dependent on the concentration of CTAB. Maximum enhancement was achieved when 0.05 mM CTAB was added, and the enhancement factor (EF) was estimated to be as large as 7.9×10^6 (a_1) for 4-ATP. The observation is attributed to classical electromagnetic (EM) response of the strongly interacting Ag nps to the optical fields when surface plasmon resonances are induced. Therefore, these nanoparticles aggregates can be "tuned" to yield maximum SERS enhancement as different concentrations of CTAB are added.

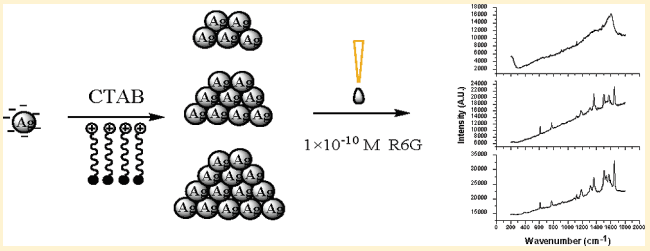

1. INTRODUCTION

Surface-enhanced Raman scattering (SERS) is a useful technique in surface chemistry and physics because of its high sensitivity and the potential in providing a great deal of information about the structures of adsorbed molecules.[1−5] Since the first observation of an intense Raman scattering from pyridine adsorbed on an electrochemically roughened silver electrode,[6] various kinds of SERS substrates have continuously arisen.[7−11] The largest SERS enhancement, even single-molecule SERS, is often present at the junction of two or more aggregated metal nanoparticles.[12−15] Xu et al. have reported that closely spaced nanoparticles separated by 1 nm can provide an enhancement of 10^{10} at the interstitial of two nanoparticles.[16] However, the extent of aggregation of metal nanoparticles is difficult to control, which is a key problem in practical analytical application of SERS. Therefore, the need for SERS substrates with good stability, high reproducibility, and remarkable enhancement factors has been well recognized in its theoretical and experimental studies.

SERS enhancement is normally described by two mechanisms, electromagnetic (EM) and chemical (CM) enhancement. EM enhancement results from the enhancement of the local electromagnetic field due to surface plasmon resonance of nanoscale surface roughness features in the 10−200 nm range.[17−20] The enhancement intensity is determined by many factors, such as size, shape, metal type, and analyte molecules adsorbed on the substrates.[21−23] A maximum enhancement factor for aggregates of nanoparticles has been reported to be up to 10^{11}.[24] CM enhancement arises from an electronic resonance charge transfer between adsorbed molecules and the metal surface with atomic-scale roughness features.[25−27] The CM enhancement contribution to the whole enhancement is estimated to be on the order of 10^2.[28] Many attempts have been paid to understand the CM process.[29,30] Recently, Tian et al. have studied the CM enhancement mechanism involved in SERS of protonated adenine adsorbed on Rh and Pd.[31]

Although EM and CM theory of SERS can simply account for all major SERS observations, a quantitative theoretical understanding of the factors affecting the SERS enhancement is still lacking. For example, the excitation of local surface plasmon (LSP) modes relates to a large enhancement of the EM field. Previous studies showed that the LSP resonance of silver or gold nanoparticle aggregates could be selectively tuned to any wavelength across the visible and the infrared regions of a spectrum by varying the size of the aggregates. However, the relationship between the degree of aggregation (or SPR) and SERS enhancement has not been studied in detail because the degree of aggregation is difficult to control.

Here, we provided a simple method to controllably fabricate Ag nps aggregates by adding different concentrations of cetyltrimethylammonium bromide (CTAB) into silver colloid. By controlling the CTAB concentration, aggregates with different sizes and LSP resonances were obtained. SERS spectra were used to investigate the SERS activity of theses aggregates, and it was found that EF can reach up to 7.9×10^6 (a_1) for 4-ATP. The Raman enhancement ability was influenced by the CTAB concentration, and the optimized SERS substrate with the largest

Received: March 29, 2011
Revised: July 11, 2011
Published: July 14, 2011

dx.doi.org/10.1021/jp205545g | J. Phys. Chem. C 2011, 115, 16295–16304

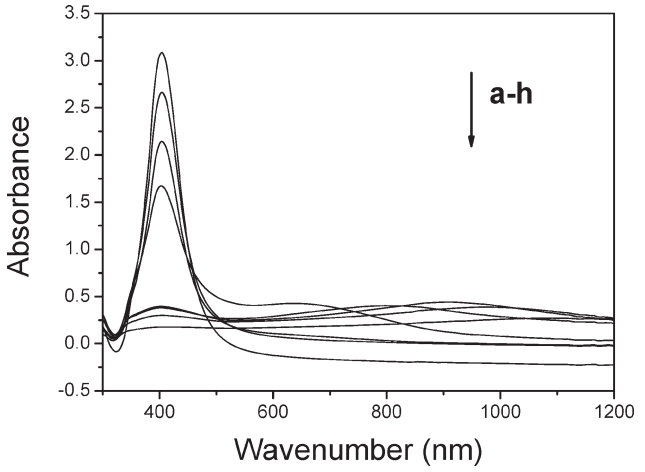

Figure 1. UV−vis absorption changes of colloidal silver with different concentrations of added CTAB solution: (a) 0, (b) 0.01, (c) 0.02, (d) 0.05, (e) 0.1, (f) 0.25, (g) 1, (h) 5 mM.

enhancement ability was prepared when the proper concentration of CTAB was added. Finally, the relationships between LSP, degree, and EF of these aggregates were discussed, and the enhancement mechanism of SERS was studied. This work indicated that CTAB plays significant role in the formation of aggregates of Ag nps, and a suitable CTAB concentration could cause the formation of an optimal SERS-active substrate with the largest enhancement. Although some noble metallic nps, such Au, Ag, Pt, and Pd nps, have been widely used for SERS applications, this work provides a new idea for investigating the effect of surfactant-induced Ag nps aggregation on the SERS enhancement.

2. MATERIALS AND METHODS

2.1. Materials. Silver nitrate ($AgNO_3$, A.R.), trisodium citrate dehydrate (A.R.), cetyltrimethylammonium bromide (A.R.), and ethanol (G.R.) were purchased from Beijing Chemical Co. (Beijing, China). Rhodamine 6G (R6G) was purchased from Exciton Chemical Co. Inv. (Dayton, OH). 4-Aminothiophenol (4-ATP) was obtained from Aldrich. All of these chemicals and materials were used as received. The water used throughout this work was ultrapure water (18.2 MΩ·cm) produced by a Milli-Q system. All of the glassware used for this experiment was washed with aqua regia and rinsed with distilled water before use.

2.2. Preparation and Characterization of Ag nps Aggregates. Silver colloids were prepared according to the standard citrate reduction of Lee and Meisal.[32] Briefly, 50 mL of a 1 mM $AgNO_3$ solution was heated with vigorous stirring to boiling; then, 1 mL of 1% trisodium citrate solution was added all at once, and vigorous stirring was continued for 1 h. Then, the colloid was cooled in air, and finally, the volume was adjusted to 50 mL with water. The prepared green−yellow silver colloid was characterized by UV−vis spectra and the zeta potential system.

Seven 1 mL samples of silver colloids were purified by centrifugation (10000 rpm, 20 min), and then, the solid portions were collected and redispersed into 2 mL of ultrapure water. To this, seven 2 mL CTAB samples, dissolved in ethanol solutions of different concentrations (0.01−5 mM, initial concnetrations) were added using a pipet, and then, 20 μL of such a mixture was dropped onto the freshly cleaved mica, left to dry in air, and then subjected to Raman analysis. It should be indicated that the surface area of the mica surface was about 1 cm^2. The mixture solution was dispersed and covered the entire mica surface, which was observed by optical microscopy (data not shown). The dispersing areas of the solutions of the R6G and 4-ATP were both about 1 cm^2, which can be indicated from SERS spectra of 20 different points on each substrate (data not shown).

2.3. SERS Measurement. R6G solution was diluted to various concentrations ranging from 1×10^{-9} to 1×10^{-14} M with ethanol, and then, 20 μL of each solution was dropped onto the SERS substrates prepared under various CTAB concentrations, and the solvent was allowed to evaporate under ambient conditions. The 4-ATP solution was diluted to 1×10^{-7} M with ethanol. Then, 20 μL of such a solution was dropped onto the SERS substrate, and the solvent was allowed to evaporate under ambient conditions. In this experiment, more than 5 SERS-active substrates of each of the silver aggregates were prepared, and 10 different points on each substrate were selected to detect the R6G and 4-ATP probes to verify the stability and reproducibility of these SERS-active substrates.

2.4. Instruments. UV−vis absorption spectra were collected in colloid using a UV-3101PC UV−vis−NIR spectrophotometer (Shimadzu, Japan). The morphology of the samples was investigated by field emission scanning electron microscopy (FESEM, Hitachi S-4800). Particle size distributions and the zeta potential were analyzed by Zeta PALS (Brookhaven Instruments Corp., Holtsville, NY). SERS spectra were measured with a T64000 Raman spectrometer from France JY Company equipped with a liquid-nitrogen-cooled CCD detector and an Ar+ gas laser (514.5 nm). The microscope attachment was based on an Olympus system, and a 50× objective was used to focus the laser beam onto a spot approximately 1 μm in diameter. The Raman band of a silicon wafer at 520 cm^{-1} was used to calibrate the spectrometer. The laser power at the sample was not more than a few mW. The spectral resolution was 0.15 cm^{-1}. The scattered light was at an angle of 180°. All of the spectra reported were the results of a single 20 s accumulation.

3. RESULTS AND DISCUSSION

3.1. Effect of CTAB Concentration on Ag nps Aggregates Size. Figure 1 shows the UV−vis absorbance spectra of synthesized silver colloid and the aggregated colloid. The silver colloid exhibits a strong plasmon band with a maximum absorbance at ~404 nm, which is similar to that reported by Graham et al.[33] When CTAB was added to the silver colloid, it revealed a distinct change for the absorbance curve; the high and sharp peak changed into a short and wide one. In addition, a new broad plasmon band at longer wavelength was present. The appearance of an extended plasmon band can be attributed to the coupling of the plasmon absorbance of the closely spaced silver nps. CTAB is usually used as a capping reagent to prepare Ag nps, and the surfactant CTAB is composed of hydrophobic and hydrophilic parts. It is suggested that the hydrophobic group (CH_3-$(CH_2)_n$−) faces silver nanoparticles, and the hydrophilic cation group (−NH_4) faces liquid phase.[34]

Figure 2a shows the SEM image of Ag nps deposited onto an ITO substrate on which the isolated and spherical nanoparticles were present. It should be noted that the ITO slide has a conductive and flat surface; thus, it was used here for ease of SEM imaging. While mica is a insolate crystal, it could not be used directly as the substrate for SEM image. Figure 2b−h shows SEM images of Ag nps aggregates formed by adding different

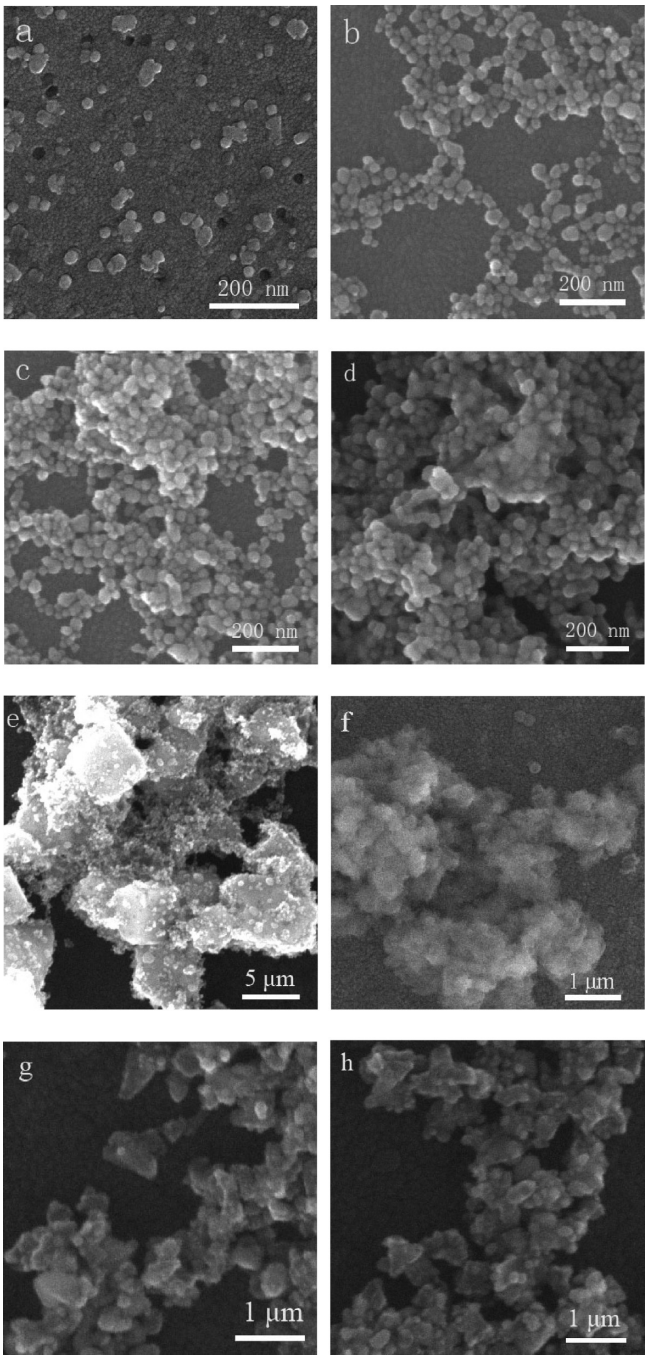

Figure 2. SEM images of corresponding Ag nps aggregates formed under different concentrations of added CTAB solution: (a) 0, (b) 0.01, (c) 0.02, (d) 0.05, (e) 0.1, (f) 0.25, (g) 1, (h) 5 mM.

concentrations of CTAB into silver colloid. It reveals that the aggregation degree increases and then decreases as more CTAB concentration is added. Zeta PALS was used to measure the sizes of the silver colloid and the CTAB-aggregated silver colloid. Figure 3a shows the statistical histogram of the size of the Ag nps, which is about 32.37 ± 0.71 nm. Figure 3b–h shows that the size of silver aggregates increases from ~49.7 nm to ~5.2 μm with different CTAB concentrations. When the added CTAB concentration was increased to 0.1 mM, a statistical analysis revealed that the diameter of the aggregates was increased to about 5.2 μm, which achieved the maximum value for the aggregates size. When the CTAB concentration was further increased (more than 0.1 mM), the size of the aggregates decreased obviously, and when the CTAB concentration was increased to 10 mM, the size of the aggregates decreased to about 132 nm (Figure 4c). However, how did silver nanoparticles aggregate and form various aggregates under different CTAB concentrations? We proposed that electrostatic interaction is the main force to cause aggregation. Trisodium-citrate-capped Ag nps are electronegative; therefore, the hydrophilic cation group ($-NH_4^+$) of CTAB can be easily bound to the surface of trisodium citrate, and this led to a partial removal of the protective trisodium citrate layer on Ag nps and resulted in the aggregation of Ag nps.

The Zeta potential measurement has been performed to support our statement of electrostatic interactions between CTAB and trisodium-citrate-capped Ag nps. The zeta potential of the as-synthesized Ag nps was ~−42.9 mV because of the presence of trisodium citrate on their surfaces. As indicated in Figure S2 (Supporting Information), the degree of negative surface charge decreased with increasing CTAB concentration over the concentration range from 0 to 0.1 mM and reached 0 at ~0.1 mM CTAB. Over the CTAB concentration range from 0.1 to 10 mM, the surface charge reversed to positive values and increased with increasing CTAB concentration. From these zeta potential results, it can be concluded that the citrate on Ag nps was first removed and then replaced by CTA^+ gradually. Therefore, the aggregation of Ag nps was induced by the CTA^+ effect. In addition, when the CTAB concentration was more than 0.1 mM, silver colloidal particles consisted of an elemental silver core surrounded by a layer of CTAB. The hydrophobic group ($CH_3(CH_2)_n-$) faced Ag nps, and the hydrophilic cation group ($-NH_4$) faced the liquid phase. The synthesis of CTAB-capped Ag nps and the interaction between CTAB and Ag nps have already been intensively investigated by Tang et al.[35] In their experiment, AgBr coproducts appeared when the CTAB concentration was larger than 0.04 M. The reaction was $Ag^+ + Br^- =$ AgBr. However, in this work, Br^- cannot interact with Ag nps to form AgBr because Ag^+ ions have already been reduced to Ag^0 and form Ag nps. From SEM and zeta potential results, it can be seen that Ag nps aggregated, and the size and aggregation degree of the Ag nps aggregation increased with the increasing CTAB concentration. Therefore, we suggested that these nanoparticle aggregates can be tuned as different concentrations of CTAB are added.

Figure 4a shows the UV–vis absorbance spectrum of the silver aggregates obtained by adding 10 mM CTAB to silver colloid. Two absorption peaks can be found in this spectrum, one narrow peak at 410 nm, corresponding to the surface plasmon resonance (SPR) peak of Ag nps, and another wide peak at 673 nm, which is attributed to the appearance of silver aggregates. The peak at 410 nm is a little weaker than the peaks shown in Figure 1a–h, which are all at about 404 nm. As we all know, the SPR wavelength of the metal nanoparticles is dependent on particle size, size distribution, and environment; on the other hand, it was reported that capping reagents could restrict the size and uniformity of nanoparticles. Cationic surfactants are excellent capping reagents to prepare stable and monodisperse positively charged metal nanoparticles for their particular characters.[36–38] Therefore, it is reasonable that the Ag nps aggregates are capped by surfactant CTAB again when the CTAB concentration is high enough. The SEM image and size distribution of Ag nps aggregates are shown in Figure 4b,c. The size of the Ag nps decreased

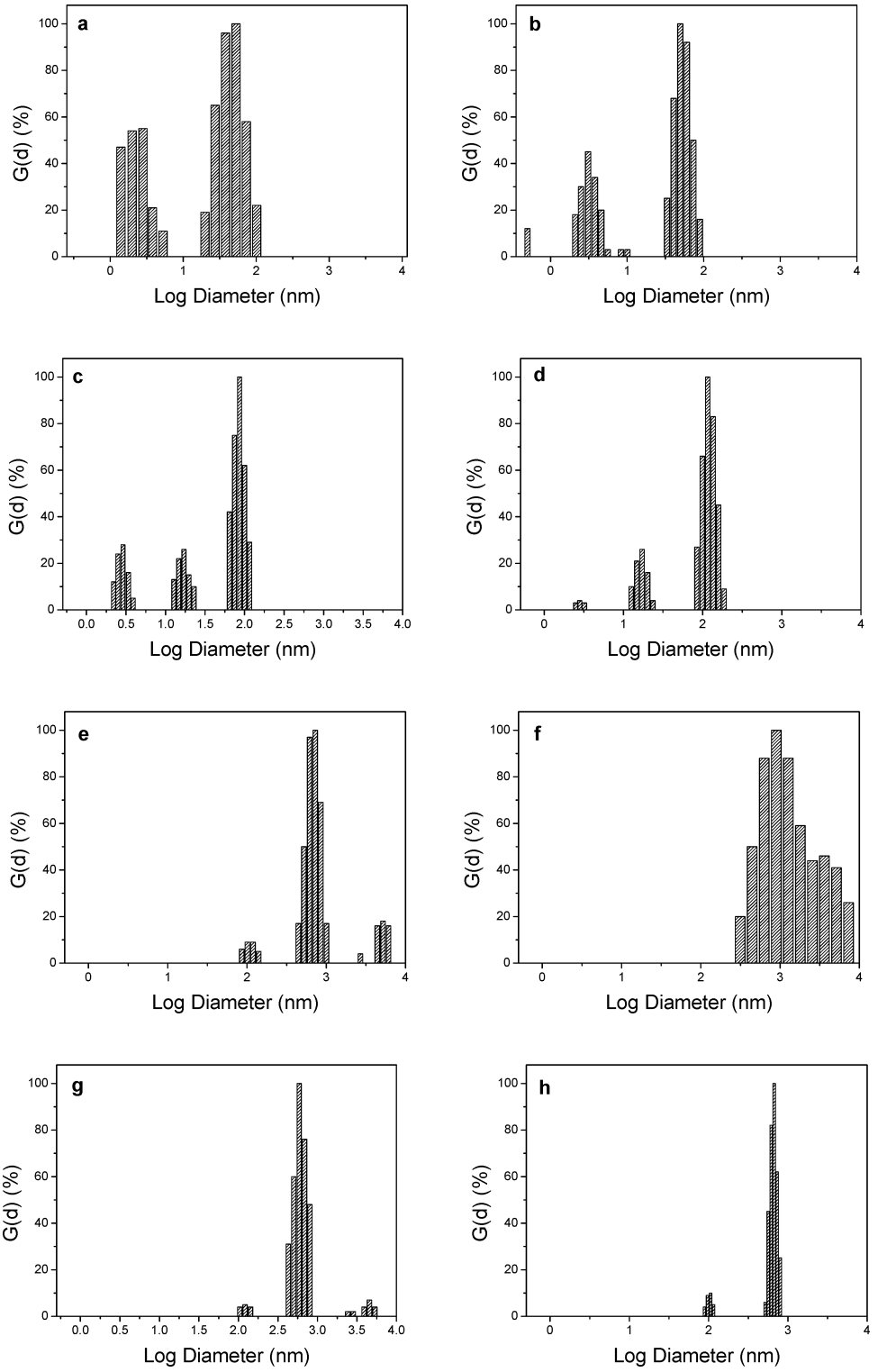

Figure 3. The size distribution histograms of corresponding Ag nps aggregates formed under different concentrations of added CTAB solution: (a) 0, (b) 0.01, (c) 0.02, (d) 0.05, (e) 0.1, (f) 0.25, (g) 1, (h) 5 mM.

obviously compared with that of Ag nps shown in Figure 2b−h. The UV absorbance peaks and size distributions of colloidal silver with different concentrations of CTAB are summarized in Table 1.

To verify the role of ethanol in the aggregation of Ag nps, a control experiment was carried out. Figure 5a and b shows the UV−vis absorbance spectrum and the size statistical histogram of silver colloid when absolute ethanol was added, respectively. Figure 5a shows little change for the absorbance curve before and after adding ethanol, which reveals that no aggregation occurs when absolute ethanol is added without CTAB. Consistent with this, the SEM image and statistical histogram of the particle size

show little change compared with that of the as-synthesized silver colloid (shown in Figure 5b,c). We have previously reported that silver aggregates could be synthesized by adding ethanol to the CTAB-capped silver colloid.[39] In the previous work, ethanol-induced aggregation was attributed to preferential dissolution of CTAB into ethanol, which led to a partial removal of the protective CTAB layer on Ag nps. Our system is significantly different from those of previous work; here, Ag nps were initially stabilized by negative citrate ions, and then, positively charged surfactant CTAB was added. CTAB balances the negative charge on the Ag nps, which brings the silver nps in close adjacently and results in aggregation of silver nps, which is similar to the study of Wei et al.[40] In their study, mica was first modified with CTAB and then immersed into silver colloid for about 2 h to obtain a SERS

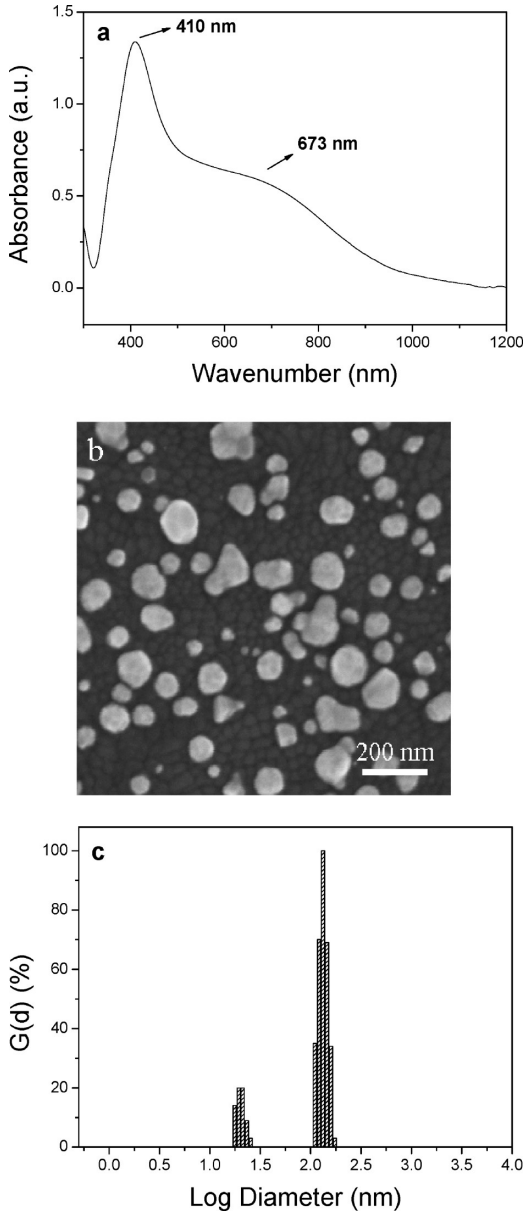

Figure 4. (a) UV−vis absorption spectrum, (b) SEM image, and (c) size distribution of Ag nps aggregates with 10 mM CTAB solution.

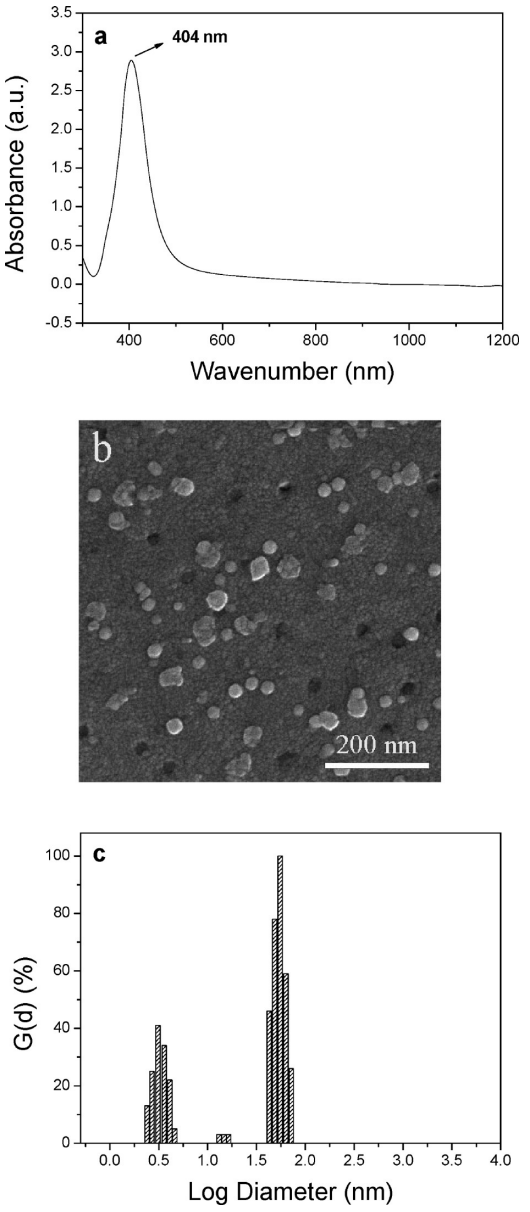

Figure 5. (a) UV−vis absorption spectrum, (b) SEM image, and (c) size distribution of Ag nps in the presence of absolute ethanol.

Table 1. UV Absorbance Peaks and Size Distributions of Colloidal Silver with Different Concentrations of CTAB: (a) 0, (b) 0.01, (c) 0.02, (d) 0.05, (e) 0.1, (f) 0.25, (g) 1, (h) 5 mM

initial concentration of CTAB (mM)	0	0.01	0.02	0.05	0.1	0.25	1	5	10
UV absorbance (nm)	404	404	404	404, 634	404, 806	404, 898	404, 982	404, 1059	410, 673
mean diameter (nm)	32.37 ± 0.71	49.72 ± 0.54	86.62 ± 0.56	116.2 ± 0.89	5207.6 ± 14.26	893.8 ± 3.62	797.2 ± 2.23	670.8 ± 1.25	132.7 ± 0.36

dx.doi.org/10.1021/jp205545g |J. Phys. Chem. C 2011, 115, 16295–16304

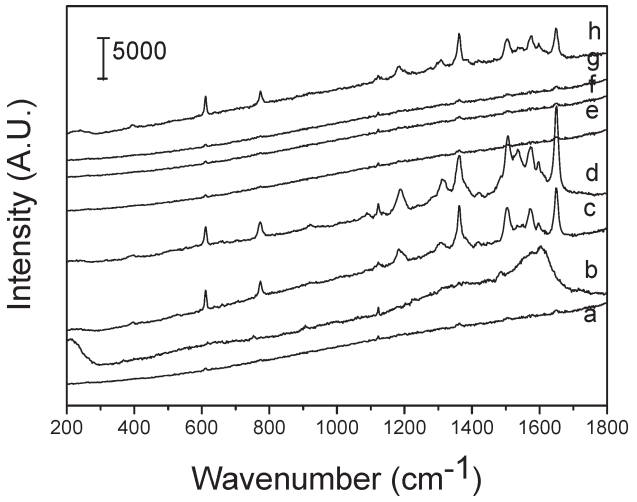

Figure 6. SERS spectra of R6G (1×10^{-10} M) on Ag nps substrates (a−h) with different concentrations of CTAB: (a) 0, (b) 0.01, (c) 0.02, (d) 0.05, (e) 0.1, (f) 0.25, (g) 1, (h) 5 mM.

substrate. However, in our work, SERS substrates could be fabricated immediately as soon as silver aggregation was induced by CTAB solution dropping onto the mica surface. From the above analysis, it is concluded that the aggregation degree and the size of aggregates can be tailored by controlling the CTAB concentration. In reference to the electromagnetic mechanism of SERS, this implies that a wavelength-dependent SERS-active substrate can be fabricated simply by adding different concentrations of CTAB into silver colloids.

3.2. Dependence of the SERS Signal on the Concentration of CTAB. We evaluated the performance of the silver aggregates as SERS substrates using R6G as a model compound. R6G is one of most common used dye molecules to characterize the SERS enhancement of silver substrates.[41−43] R6G samples of ultralow concentration were used to verify the dependence of the enhancement effect of this SERS-active substrate on the CTAB concentration. The Raman signal of R6G molecules partially contributes to the resonance enhancement (about 2−3 orders of magnitude) of the laser used, such as the 514.5 nm argon ion laser used in this work; therefore, the spectrum of R6G detected is actually the surface-enhanced resonance Raman scattering (SERRS) signal. From the above analysis of optical properties and size distributions, we deduced that these silver aggregates prepared under different concentrations of CTAB should have different SERRS intensities for R6G molecules. Figure 6 shows a set of SERRS spectra of 1×10^{-10} M R6G on the Ag nps aggregates with different concentrations of CTAB. Upon increasing the concentration of CATB, a subsequent intensification of the signal is observed due to the formation of Ag nps aggregates showing more appropriate morphological properties to induce an intense local electric field through SPR. As expected from the UV−vis spectra, the SERS peaks from the 116.2 nm silver aggregates are very intense (Figure 6d). On this substrate, R6G produced a clear enhanced effect at 1650 cm^{-1}, which was one of the main characteristic bands. The Raman peaks at 612 (C−C−C ring), 769 (C−H bend), 1128 (C−H bend), 1188, 1315, 1357 (aromatic C−C stretching), 1505 (aromatic C−C stretching), 1573 (aromatic C−C stretching), and 1650 cm^{-1} (aromatic C−C stretching) are characteristic vibrations of R6G.[44] An obvious trend is that the enhancement ability increases strongly with the

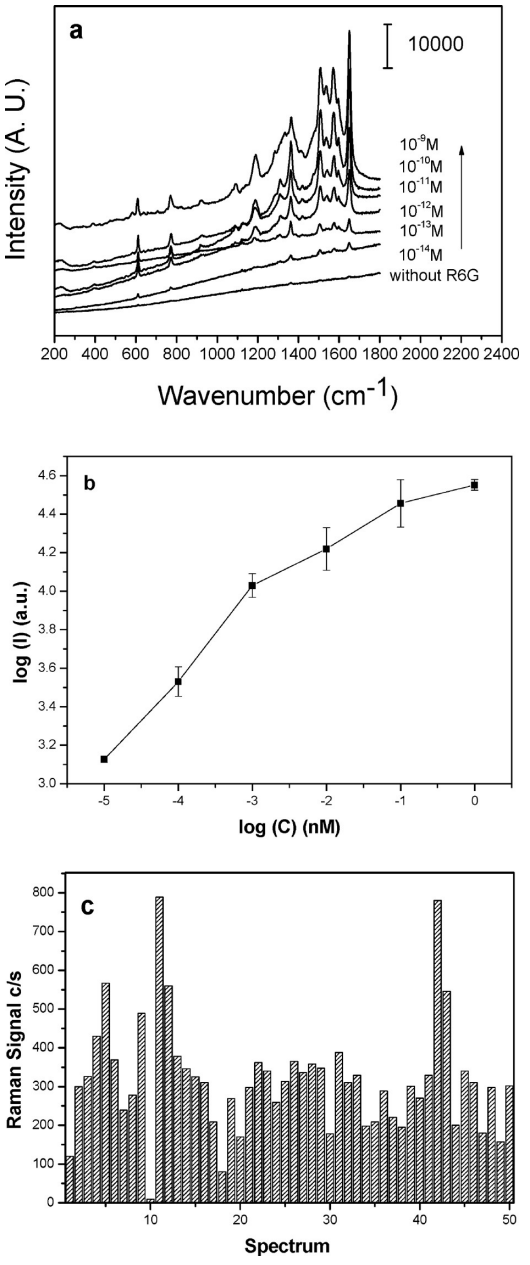

Figure 7. (a) SERS spectra of R6G of various concentrations on an active substrate. (b) The intensity (log(I)) of SERS signal at 1650 cm^{-1} under various concentrations (log(C)) of R6G. (c) Peak height of the 1650 cm^{-1} line for the 50 SERS spectra obtained when the concentration of R6G was 1×10^{-10} M. Power: 25 mW, 1%; integration time: 30 s.

increase of CTAB concentration, and it will achieve the maximum enhancement when the CTAB concentration reaches 0.05 mM. However, the SERRS signal observed decreases when the CTAB concentration exceeds 0.05 mM, and a weak SERRS signal appears again when the CTAB concentration reaches 5 mM. In summary, under the same experiment conditions (integration time: 20 s; power: 1%), 0.05 mM CTAB-induced aggregates revealed greater SERS signal than other aggregates induced by a different CTAB concentration. Therefore, 0.05 mM CTAB-induced aggregates were used as the SERS substrate in the following experiments.

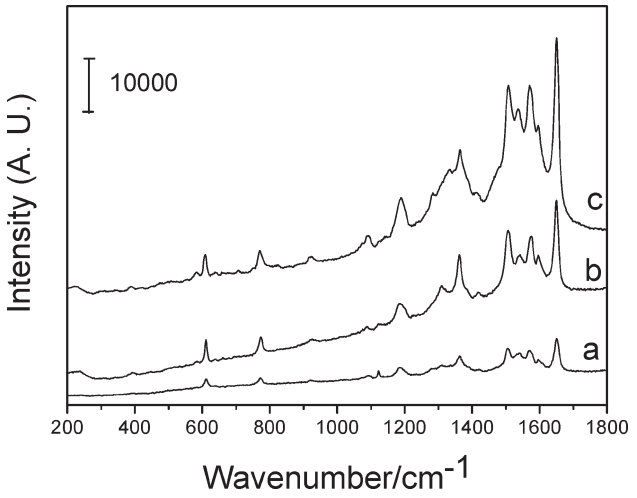

Figure 8. SERS spectra of R6G (1×10^{-9} M) on the active substrate d: (a) initially prepared, (b) after 1 months of storage, and (c) after 2 months of storage.

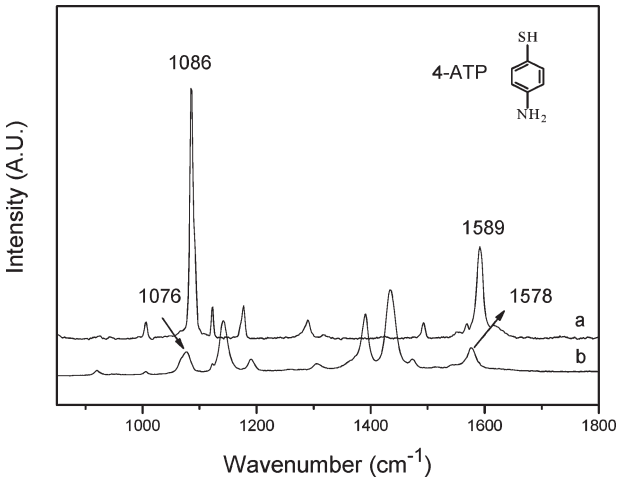

Figure 9. Comparison of a normal Raman spectrum and a SERS spectrum of 4-ATP: (a) normal Raman spectrum of solid 4-ATP and (b) SERS spectrum of 4-ATP (1×10^{-7} M) on the active substrate d.

3.3. Dependence of the SERRS Signal on the Concentration of R6G and the Stability of the Substrate. Figure 7a shows the typical SERRS spectra of R6G with various concentrations ranging from 1×10^{-9} to 1×10^{-14} M. A 20 μL R6G ethanol solution was dropped on the silver substrates, and the solvent was allowed to evaporate under ambient conditions. Then, the SERS spectra were collected as soon as the R6G solution was dried. It should be noted that R6G molecules will desorb from the surface during the storage for a long time, leading to a decrease of the SERS signal. Figure 7b shows the relationship between the R6G concentration and the intensity in a $\log(I)-\log(C)$ style plot of the SERRS signal at 1650 cm^{-1}, in which the background of the signal has been removed in drawing the graph. It shows that the peak intensity increases nonlinearly with the concentration when the R6G concentration exceeds 1×10^{-13} M. This nonlinear dependency relationship reveals that the adsorption of R6G onto adsorption sites with high enhancement (hot spots) becomes saturated beyond this level. Therefore, we can conclude that R6G was not adsorbed onto the SERS-active substrate averagely but adsorbed onto the hot spots provided by aggregates. The relationship between the Raman peak intensity and the R6G concentration was similar to that was reported by Wang et al., who investigated the SERS spectra of R6G molecules on silver nanoparticle arrays with tunable sub-10 nm gaps.[45] To examine the reliability of the optimal substrate, SERS (50 numbers) spectra of R6G (1×10^{-10} M) were also obtained. Figure 7c displays the peak heights of the 1650 cm^{-1} line for the 50 SERS spectra. In the histogram, 39 of the 50 spectra show a great Raman signal (>200 c/s), and only one spectrum shows low Raman signal (<10 c/s). Because the selection of the location measured is random, we conclude that this substrate is reliable.

The stability of the substrates was investigated by detecting the Raman activity over time. The substrates could give a Raman signal even 2 months after they were drop-coated with R6G molecules. Figure 8 shows the aging of SERRS spectrum for R6G (1×10^{-9} M) on Ag nps aggregates. The SERRS intensity decreases over a period of 2 months, but the characteristic bands of R6G are still clear, which meets the basic demands of analytical researches. We think that the reduction of the intensity is attributed to two main causes; one cause is the R6G desorption on the SERS-active sites, and the other cause is the decay of the activity of the silver nanoparticles. Therefore, the SERS substrate prepared with our method has good stability.

When dropping silver nanoparticles onto the cleaved mica directly, the SERS spectrum shows that the lowest detectable concentration of R6G is only about 1×10^{-9} M on this substrate; moreover, the stability and reproducibility are poor. However, for 0.05 mM CTAB-induced Ag aggregates, the greatest enhancement effect is observed, and the limit of detection is up to 1×10^{-14} M. Even if we reduced the laser power to 1%, an interpretable Raman signal was still obtained (data not shown). Therefore, we concluded that the aggregation extent of the silver colloid could affect SERS signals greatly.

3.4. Estimation of the SERS Enhancement of Different Ag nps Aggregates. We evaluated the performance of Ag nps aggregates as SERS substrates using 4-ATP as a model compound. 4-ATP is composed of a benzene ring, $-SH$, and $-NH_2$, and its structure is shown in the inset of Figure 9. Figure 9 shows the normal Raman spectrum of solid 4-ATP (Figure 9a) and the SERS spectrum of 4-ATP on this SERS-active substrate (Figure 9b). The normal Raman spectrum of solid 4-ATP is similar to that reported by Osawa et al. and Zheng et al.[46,47] Compared with the spectrum obtained in the solid, the noticeable differences in the SERS spectrum are the frequency shifts for some changes in band intensity. The obvious Raman frequency shifts from 1086 cm^{-1} (a_1) in Figure 9a to 1076 cm^{-1} (a_1) in Figure 9b. We have attempted to estimate the SERS enhancement factor(EF) by using the following relationship

$$EF = (I_{SERS}/I_{Raman})(M_{bulk}/M_{surface})$$

where I_{SERS} and I_{Raman} are the SERS intensity of 4-ATP on Ag nps aggregates and the normal Raman scattering intensity of 4-ATP in bulk, respectively; M_{bulk} is the concentration of molecules in the bulk sample, and $M_{surface}$ is the concentration of adsorbed molecules. I_{SERS} and I_{Raman} were both measured at 1076 cm^{-1} (a_1), and $M_{surface}$ and M_{bulk} were calculated on the basis of the estimated concentration of surface 4-ATP species, the density of bulk 4-ATP, and the sampling areas. For the target molecule 4-ATP, in the sample area (1 μm in diameter) measured, $M_{surface}$ was calculated to be 1.2×10^{12} /cm^2. Taking

the laser spot (1 μm in diameter) and the penetration depth (about 2 μm) and the density of 4-ATP (1.17 g/mL) into account,[41] M_{bulk} had a value of 0.82×10^{18} /cm^2 in the detected solid sample area. For the vibration modes at 1076 cm^{-1} (a_1), an EF of 7.9×10^6 was obtained. Etchgoin and Tian's groups have comprehensively studied the SERS enhancement factor in their review papers.[48,49] For the penetration depth of the focused laser beam, different experiments have different values. For example, Wang et al. have estimated the penetration depth to be about 16.5 μm;[50] Li et al. have estimated the penetration depth to be about 2 μm.[41] This value depends very much on the optical quality of the solid and the preparation method. During estimation of EF values, the laser spot and the penetration depth are both assumed by researches, and in most cases, the laser spot and the penetration depth are assumed to be 1 and 2 μm, respectively, for silver colloids. As the laser probing spot is very small and the heat transfer becomes obvious, therefore, repeated laser pulsing can drills a hole into the surface. Here, atomic force microscopy (AFM) was used to estimate the penetration depth by imaging the hole, and the penetration depth was estimated to be about 2 μm (see Figure S1, Supporting Information). Suppose that 4-ATP solution is dispersed on the surface uniformly and then the density of the 4-ATP on the surface is assumed to be 10^{-7} M $\times$ 20 μL $\times$ N_A /cm^2 (the surface area of the substrate is 1 $\times$ 1 cm^2; N_A is 6.02×10^{23}), namely, 1.2×10^{12} /cm^2. It is well-known that for a small molecule, the surface concentration is about $10^{14}-10^{15}$/cm^2. The concentration of 4-ATP molecules was less than this value, but we could still gain a clear SERS spectrum. Therefore, we can conclude that 4-ATP was not absorbed to the SERS-active substrate averagely but absorbed to the hot spots provided by aggregates.

The EF value is dependent on the type of probe molecule, laser power, wavelength of laser, and type of vibrations. First, different probe molecule shows different enhancement for SERS. For 4-ATP, the EF values were usually reported to be 10^4-10^6 (a_1) and 10^5-10^{10} (b_2),[51] and the EF value for the a_1 mode is usually lower than that for the b_2 mode. Second, the EF values increase with the increasing laser power. In this work, the laser power on the substrate is lower than 0.25 (25$\times$1%) mW, which is far below the laser power (10 mW) reported in ref 52. Third, the wavelength of the laser is a key factor for SERS enhancement. For example, Wang et al. have reported that EF values were different for different wavelengths (514.5, 794.4, and 1064 nm excitations).[52] Finally, the EF value estimated by the formula mentioned above is smaller than those from other calculation methods.[53]

The EF values of the other Ag nps aggregates have been estimated according to a method similar to that mentioned above and are indicated in Table 2. Comparing the EF values on the different substrates, it can be seen clearly that the enhancement of 0.05 mM CTAB-induced aggregates is more than 20 times larger than the other different aggregates induced by different concentrations of CTAB. This further indicates that the SERS intensity was dependent on the size of Ag nps aggregates. It is noted that 1589 cm^{-1} (b2) was always used to estimate the EF value, but Tian et al. have already pointed out that the signal is not from 4-ATP but a new species produced under the illumination of the laser.[54] Therefore, 1589 cm^{-1} (b2) is not used here to estimate the EF value.

It should be noted that the forms of 4-ATP in the solid and in the adsorption state are different. As mentioned above, the S−H band of 4-ATP in the adsorption state changed to the Ag−S band, which has been proven by the ν_{CS} band shift from 1086 cm^{-1} in Figure 9a to 1076 cm^{-1} in Figure 9b. The ATP molecule is a usually used probe molecule to quantitatively estimate the enhancement effect of different silver nanostructures.[41−43,55] For example, Wang et al. estimated the EF values by comparing the Raman spectrum of solid *p*-ATP and SERS of adsorbed *p*-ATP on silver nanoplates.[42] Hou et al. have estimated the EF values by comparing the Raman spectrum of solid 4-ATP and SERS of adsorbed 4-ATP on hydrophobic and hydrophilic Ag nanoparticles.[55] They both found the Ag−S band when ATP molecules were adsorbed on the silver surface.

Table 2. UV Absorbance Peak (nm), Mean Diameter, and Corresponding EF Values for Ag nps Aggregates

		EF (enhancement factor)
UV absorbance (nm)	mean diameter (nm)	1075 cm^{-1} (a_1)
404	32.37 ± 0.71	
404	49.72 ± 0.54	
404	86.62 ± 0.56	3.2×10^5
404, 634	116.20 ± 0.89	7.9×10^6
404, 806	5207.61 ± 14.26	
404, 898	893.81 ± 3.62	
404, 982	797.27 ± 2.23	
404, 1059	670.84 ± 1.25	2.7×10^4

3.5. Aggregation Degree Is the Main Factor for the SERS Enhancement. We suggest that the size and aggregation degree of Ag nps aggregates are two main factors for the enhancement ability of SERS. It can be seen from Table 2 that the size of the Ag nps aggregates first increased and then decreased with the increase of CTAB concentration. The SERS intensity was found to be strongest for R6G adsorbed on surfaces covered with 116.2 nm Ag nps aggregates. For this aggregate, an extended plasmon band appeared (shown in Figure 1d), which indicates the decrease in interparticle separation. Thus, in the Ag nps (116.2 nm) aggregates, the number of "hot junctions" increases and provide a much more intense SERS band. According to Nie's studies about single molecules, they found that the greatest SERS enhancement occurs at the junction between two metal nanoparticles.[56] As the size of the aggregates increases, the number of "junctions" increases and thus provides a more intense SERS enhancement. Classical electromagnetic theory predicted that the enhanced fields around each nanoparticle can interfere coherently.[57] As the distance between the nanoparticles decreases, the coupled plasmon resonance shifts to the red, and the enhanced electromagnetic field increases in the junction of the aggregated nanoparticles. The junction thus can be considered as an electromagnetic "hot spot" similar to those predicted to exist in large aggregates of Ag nps.[58] From this result, we can conclude that the enhancement is due to the electromagnetic effect. The enhancing ability is then understood to have a bearing with field enhancement that originates from electromagnetic interactions among the constituents of Ag nps in the aggregates. By comparing the sizes with SERS EF values of aggregates, it can be concluded that ~116.2 nm is the best size for SERS enhancement.

On the other hand, the effect of SPR on the EF values should be considered. The highest EM field enhancement arises when the irradiation wavelength is resonant with the SPR maximum.[59,60] For SERS measurements, a 514.5 nm laser was used; therefore, one could expect to see enhanced SERS activity for these Ag nps aggregates with more red-shifted SPR bands. For 116.2 nm Ag

nps aggregates, the SERS intensity was greatly enhanced as the SPR band of these Ag nps aggregates was red shifted. However, the strong activity of 670 nm Ag nps aggregates is hard to understand because the Ag nps aggregates have the most red-shifted SPR (1059 nm) but the weakest enhancement (as shown in Table 2). This observation suggests that although the position of the SPR band relative to the laser wavelength is important for SERS, there may be other significant factors to the enhancement mechanism such as the above-mentioned aggregation degree. Etchegoin et al. have shown that the resonances of the hot spots do not coincide with the SPR measured by UV−vis spectroscopy.[61] Therefore, the close degree between SPR and the excited wavelength cannot be used as a sole criterion for maximum enhancement. A systematic investigation, such as the one presented here, is then important to understand the SERS enhancement mechanism.

From the experimental results, it is revealed that the uneven size distribution of the aggregates would not influence the reproducibility. From Figure 2b−d, it can be seen that the aggregation degree of Ag nps increased, and the multidimensional and multilayer structures formed. With the diameter of isolated nanoparticles in mind, Figure 2b presents 1−2 layer Ag nps aggregates, whose diameters are about 1−2 times that of single Ag nps. Figure 2c presents 2−3 layers of stacked Ag nps, and Figure 2d presents 3−4 layers of stacked Ag nps. By comparing the SEM images of the Ag nps aggregates with their corresponding SERS spectra, it was found that aggregates with more layers of stacked nps show greater SERS enhancement. Similar results have been reported by Pignataro et al., and they found that the multilayer stacked nps exhibited greater SERS enhancement than aggregates limited to two-dimensional or one-dimensional structures and suggested that the dimensions for surface protrusions are crucial in determining the intensity of SERS enhancement.[62] Therefore, we can gain insight into the relationship between the dimension of Ag nps aggregates and the intensity of SERS enhancement in terms of the electromagnetic mechanism (EM). As stated by Sun et al., the SERS effect is mainly related to the interaction between closely stacked nps that induces a perturbation of the local electromagnetic field around each nanoparticle.[63] The perturbation of the electromagnetic field among the closely stacked Ag nps increases the intensity of the electromagnetic field. Thus, it can be included that the SERS enhancement is caused by the increase of the local electromagnetic field of the aggregates with closely stacked nps. Therefore, larger SERS enhancement could be achieved at the aggregates with more layers of stacked Ag nps due to the enormous electromagnetic field. From the above discussions, it is reasonable to conclude that electromagnetic field enhancement plays an important role in the SERS enhancement.

4. CONCLUSIONS

A variety of Ag nps aggregates have been obtained by adding different concentrations of CTAB into silver colloid and were characterized by UV−vis spectroscopy and zeta potential measurement. Substrates of each type of the Ag nps aggregates were prepared and used for SERS measurements with a confocal Raman microscope. In general, 116.2 nm Ag nps aggregates give greater SERS enhancements than other aggregates of different sizes. There was a strong correlation between the SERS intensity and the size or aggregation degree of the aggregates. The SERS enhancement is attributed to great contributions from the EM enhancement due to SPR and aggregation degree, which is indicated by the relationship between SERS activity and SPR position of the aggregates.

■ ASSOCIATED CONTENT

Supporting Information. AFM image of surface damage by Raman and the zeta potential for citrate−AG nps solutions. This material is available free of charge via the Internet at http://pubs.acs.org.

■ AUTHOR INFORMATION

Corresponding Author
*E-mail: dxzhao2000@yahoo.com.cn.

■ ACKNOWLEDGMENT

This work was supported by China Postdoctoral Science Foundation No. 20100481068.

■ REFERENCES

(1) Michaels, A. M.; Jiang, J.; Brus, L. *J. Phys. Chem. B* **2000**, *104*, 11965.
(2) Tao, A.; Kim, F.; Hess, C.; Goldberger, J.; He, R. R.; Sun, Y. G.; Xia, Y. N.; Yang, P. D. *Nano Lett.* **2003**, *3*, 1229.
(3) Faulds, K.; Smith, W. E.; Graham, D. *Anal. Chem.* **2004**, *76*, 412.
(4) Andrade, G. F. S.; Temperini, M. L. A. *J. Phys. Chem. C* **2007**, *11*, 13821.
(5) Papadopoulou, E.; Bell, S. E. J. *Analyst* **2010**, *135*, 3034.
(6) Fleischmann, M.; Hendra, P. J.; McQuillan, A. J. *Chem. Phys. Lett.* **1974**, *26*, 163–6.
(7) Cui, Y.; Ren, B.; Yao, J. L.; Gu, R. A.; Tian, Z. Q. *J. Phys. Chem. B* **2006**, *110*, 4002.
(8) Iwanabe, Y.; Fujimaki, M.; Awazu, K.; Horiuchi, T; Tominaga, J. *Nanotechnology* **2006**, *17*, 1717.
(9) Hu, J. W.; Zhao, B.; Xu, W. Q.; Fan, Y. G.; Li, B. F.; Ozaki, Y. *Lagmuir* **2002**, *18*, 6839.
(10) Wang, Y. Z.; Li, Y. X.; Yang, S. T.; Zhang, G. L.; An, D. M.; Wang, C.; Yang, Q. B.; Chen, X. S.; Jing, X. B.; Wei, Y. *Nanotechnology* **2006**, *13*, 3304.
(11) Lu, L. H.; Eychmüller, A.; Kobayashi, A.; Hirano, Y.; Yoshida, K.; Kikkawa, Y.; Tawa, K.; Ozaki, Y. *Langmuir* **2006**, *22*, 1605.
(12) Lu, L. H.; Zhang, H. J.; Sun, G. Y.; Xi, S. Q.; Wang, H. S. *Langmuir* **2003**, *19*, 9490.
(13) Caro, C.; Lopez-Cartes, C.; Zaderenko, P.; Mejias, J. A. *J. Raman Spectrosc.* **2008**, *39*, 1162.
(14) Schwartzberg, A. M.; Grant, C. D.; Wolcott, A.; Talley, C. E.; Huser, T. R.; Bogomolni, R.; Zhang, J. Z. *J. Phys. Chem. B* **2004**, *108*, 19191.
(15) Li, Y. S.; Su, H. M.; Wong, K. S.; Li, X. Y. *J. Phys. Chem. C* **2010**, *114*, 10463.
(16) Zhou, D. S.; Li, L. A.; Xue, G.; Ge, J. J.; Xue, C. C.; Cheng, S. Z. D. *Langmuir* **2002**, *18*, 4559.
(17) McMahon, J. M.; Henry, A. I.; Wustholz, K. L.; Natan, M. J.; Freeman, R. G.; Van Duyne, R. P.; Schatz, G. C. *Anal. Bioanal. Chem.* **2009**, *394*, 1819.
(18) Addison, C. J.; Brolo, A. G. *Langmuir* **2006**, *22*, 8696.
(19) Kahl, M.; Voges, E. *Phys. Rev. B* **2000**, *61*, 14078.
(20) McFarland, A. D.; Young, M. A.; Dieringer, J. A.; Vanduyne, R. P. *J. Phys. Chem. B* **2005**, *109*, 11279.
(21) Mclellan, J. M.; Xiong, Y. J.; Hu, M.; Xia, Y. N. *Chem. Phys. Lett.* **2006**, *417*, 230.
(22) Christopher, J. A.; Alexandre, G. B. *Langmuir* **2006**, *22*, 8696.
(23) Hu, J. W.; Li, J. F.; Ren, B.; Wu, D. Y.; Sun, S. G.; Tian, Z. Q. *J. Phys. Chem. C* **2007**, *111*, 1105.

(24) Lee, S. J.; Morrill, A. R.; Moskovits, M. *J. Am. Chem. Soc.* **2006**, *128*, 2200.
(25) Vidal, G.; Pendry, J. B. *Phys. Rev. Lett.* **1996**, *77*, 1163.
(26) Lombardi, J. R.; Brike, R. L.; Lu, T.; Xu, J. *J. Chem. Phys.* **1986**, *84*, 4174.
(27) Otto, A.; Billmann, J.; Eickmans, J.; Erturk, U.; Pettenkofer, C. *Surf. Sci.* **1984**, *138*, 319.
(28) Otto, A.; Mrozek, I.; Grabhorn, H.; Akemann, W. *J. Phys.: Condens. Matter* **1992**, *4*, 1143.
(29) Shegai, T.; Vaskevich, A.; Rubinste, I.; Haran, G. *J. Am. Chem. Soc.* **2009**, *131*, 14390.
(30) Zhao, L.; Jensen, L.; Schatz, G. C. *J. Am. Chem. Soc.* **2006**, *128*, 2911.
(31) Cui, L.; Wu, D. Y.; Wang, A.; Ren, B.; Tian, Z. Q. *J. Phys. Chem. C* **2010**, *114*, 16588.
(32) Lee, P. C.; Meisel, D. *J. Phys. Chem.* **1982**, *86*, 3391.
(33) Graham, D.; Smith, W. E.; Linacre, A. M. T.; Munro, C. H.; Watson, N. D.; White, P. C. *Anal. Chem.* **1997**, *69*, 4703.
(34) Sun, L. L.; Song, Y. H.; Wang, L.; Guo, C. L.; Sun, Y. J.; Liu, Z. L.; Li, Z. *J. Phys. Chem. C* **2008**, *112*, 1415.
(35) Fang, Z.; Tang, K. B.; Lei, S. J.; Li, T. W. *Nanotechnology* **2006**, *17*, 3008.
(36) Chen, D. H.; Hsieh, C. H. *J. Mater. Chem.* **2002**, *12*, 2412.
(37) Swami, A.; Kumar, A.; Sastry, M. *Langmuir* **2003**, *19*, 1168.
(38) Yang, Y.; Matsubara, S.; Nogami, M.; Shi, J. L.; Huang, W. M. *Nanotechnology* **2006**, *17*, 2821.
(39) Sun, L. L.; Song, Y. H.; Wang, L.; Guo, C. L.; Sun, Y. J.; Liu, Z. L.; Li, Z. *J. Phys. Chem. C* **2008**, *112*, 1415.
(40) Wei, G.; Zhou, H. L.; Liu, Z. G.; Li, Z. *Appl. Surf. Sci.* **2005**, *240*, 260–267.
(41) Wang, Y. L.; Zou, X. Q.; Ren, W.; Wang, W. D.; Wang, E. K. *J. Phys. Chem. C* **2007**, *111*, 3259.
(42) Wei, G.; Wang, L.; Liu, Z. G.; Song, Y. H.; Sun, L. L.; Yang, T.; Li, Z. *J. Phys. Chem. B* **2005**, *109*, 23941.
(43) Kneipp, K.; Kneipp, H.; Itzkan, I.; Dasari, R. R.; Feld, M. S. *Chem. Rev.* **1999**, *99*, 2957.
(44) Wang, H. H.; Liu., C, Y.; Wu, S. B.; Liu, N. W.; Peng, C. Y.; Chan, T. H.; Hsu, C. F.; Wang, J. K.; Wang, Y. L. *Adv. Mater.* **2006**, *18*, 491.
(45) Zheng, J.; Li, X.; Gu, R.; Lu, T. *J. Phys. Chem. B* **2002**, *106*, 1019.
(46) Osawa, M.; Matsuda, N.; Yoshll, K.; Uchida, I. *J. Phys. Chem.* **1994**, *98*, 12702.
(47) Lu Ru, E. C.; Blackie, E.; Meyer, M.; Etchegion, P. G. *J. Phys. Chem. C* **2007**, *111*, 13794–13803.
(48) Lin, X. M.; Cui, Y.; Xu, Y. H.; Ren, B.; Tian, Z. Q. *Anal. Bioanal. Chem.* **2009**, *394*, 1729.
(49) Moskovits, M.; Suh, J. S. *J. Phys. Chem.* **1984**, *88*, 5526.
(50) Wang, Y. L.; Chen, H. J.; Dong, S. J.; Wang, E. K. *J. Chem. Phys.* **2006**, *124*, 074709.
(51) (a) Wang, Y. L.; Chen, H. J.; Dong, S. J.; Wang, E. K. *J. Chem. Phys.* **2006**, *125*, 044710. (b) Hu, X. G.; Wang, T.; Wang, L.; Dong, S. J. *J. Phys. Chem. C* **2007**, *111*, 6962.
(52) Wang, Y. L.; Guo, S. J.; Chen, H. J.; Wang, E. K. *J. Colloid Interface Sci.* **2008**, *318*, 82.
(53) LeRu, E. C.; Etchegoin, P. G. *J. Phys. Chem. B* **2007**, *111*, 12794.
(54) Huang, Y. F.; Zhu, H. P.; Liu, G. K.; Wu, D. Y.; Ren, B.; Tian, Z. Q. *J. Am. Chem. Soc.* **2010**, *132*, 9244.
(55) Hou, X. M.; Zhang, X. L.; Chen, S. T.; Fang, Y.; Yan, J. L.; Li, N.; Qu, P. X. *Appl. Surf. Sc* **2011**, *257*, 4935.
(56) Doering, W. E.; Nie, S. *J. Phys. Chem. B* **2002**, *106*, 311.
(57) Maruyama, Y.; Ishikawa, M.; Futamata, M. *Chem. Lett.* **2001**, *30*, 834.
(58) Schatz, G. C. *Acc. Chem. Res.* **1984**, *17*, 370.
(59) Inoue, M.; Ohtaka, K. *J. Phys. Soc. Jpn.* **1983**, *52*, 3853.
(60) Halas, N. *MRS Bull.* **2005**, *30*, 362.
(61) Etchegoin, P.; Cohen, L. F.; Hartigan, H.; Brown, R. J. C.; Milton, M. J. T.; Gallop, J. C. *J. Chem. Phys.* **2003**, *119*, 5281.
(62) Pignataro, B.; Bonis, A. D.; Compagnini, G.; Sassi, P.; Cataliotti, R. S. *J. Chem. Phys.* **2000**, *113*, 5947.
(63) Xiao, T.; Ye, Q.; Sun, L. *J. Phys. Chem. B* **1997**, *101*, 632.